Production cross sections of ground and isomeric states in the reaction systems ^{93}Nb+^{3}He, ^{92}Mo+α, and ^{94,95}Mo+p

B. Strohmaier
Institut für Radiumforschung und Kernphysik, University of Vienna, Boltzmanngasse 3, A-1090 Vienna, Austria

M. Faßbender and S. M. Qaim
Institut für Nuklearchemie, Forschungszentrum Jülich GmbH, D-52425 Jülich, Germany
(Received 6 February 1997)

Cross-section measurements on the production of ^{94}Tc^{m} in the reactions ^{93}Nb(^{3}He,2n), ^{92}Mo(α,x), and ^{94}Mo(p,n) were performed recently at Jülich in order to investigate ways of producing this radioisotope on a large scale for nuclear medical application. Those experiments also yielded the excitation functions for the reactions ^{93}Nb(^{3}He,xn)^{95,94,93}Tc^{m,g} (x=1,2,3), ^{93}Nb(^{3}He,x)^{93}Mo^{m}, ^{93}Nb(^{3}He,x)^{92}Nb^{m} and ^{93}Nb(^{3}He,x)^{89}Zr^{m+g}, ^{92}Mo(α,xn)^{95,94}Ru (x=1,2), ^{92}Mo(α,x)^{94}Tc^{m,g}, and ^{92}Mo(α,p)^{95}Tc^{g} as well as ^{94}Mo(p,xn)^{94,93}Tc^{m,g} (x=1,2). A theoretical study, employing the Hauser-Feshbach and the exciton-model formalism, was now undertaken to describe the cross sections of all those reactions. The data base was supplemented by cross sections retrieved from the literature, including the reactions ^{93}Nb(^{3}He,4n)^{92}Tc, ^{92}Mo(α,p)^{95}Tc^{m}, ^{92}Mo(α,x)^{93}Tc^{m,g}, and ^{95}Mo(p,n)^{95}Tc^{m,g}. As the reactions investigated have many of the product nuclei in common, they permit the study of cross sections, in particular for the formation of pairs of isomeric states, as functions of projectile type and energy, with the cross sections for formation of nuclei via competing reactions posing additional constraints on the model parameters. Considering the rather large scatter among the experimental data sets, as well as the fact that attempts were made to describe simultaneously 25 excitation functions and 8 isomeric cross-section ratios [$\sigma^{m}/(\sigma^{m}+\sigma^{g})$] with one consistent set of model parameters, the degree of agreement achieved between experimental and calculated quantities is remarkable. In ^{3}He-induced reactions, the adoption of a spin distribution of the level population in preequilibrium emission different from that at the equilibrium stage yielded some improvement in the description of the isomeric ratios for ^{95,94,93}Tc production. [S0556-2813(97)03611-X]

PACS number(s): 25.40.−h, 25.55.−e, 24.10.−i

I. INTRODUCTION

Measurement of isomeric cross sections by means of radiochemical techniques has been a long-standing and successful scientific program at the Forschungszentrum Jülich [1]. Apart from the fundamental scientific interest in these cross sections, they also find practical applications in estimation of radioactivity in fusion-reactor design and in purity considerations in the production of medically important radionuclides. The latter is particularly true for ^{94}Tc^{m} which is discussed as a β^{+} emitting isotope of technetium suitable for quantifying the uptake kinetics of ^{99}Tc^{m} radiopharmaceuticals. Therefore, it is desirable to produce this radioisotope in high yields and with high radionuclidic purity. This could be achieved via the reactions ^{93}Nb(^{3}He,2n), ^{92}Mo(α,$np+pn+d$), and ^{94}Mo(p,n) using enriched Mo targets rather than using protons and deuterons on natural molybdenum. Comparative investigations on these production routes are described in Refs. [2–5]. Those publications also contain cross sections for the production of the ground state ^{94}Tc^{g} as well as of various other product nuclei. The measured excitation functions for ^{93}Nb(^{3}He,x)^{93}Mo^{m}, ^{93}Nb(^{3}He,x)^{92}Nb^{m}, and ^{93}Nb(^{3}He,x)^{89}Zr^{m+g} are presented here.

For an interpretation of the experimentally determined cross sections in this energy range, usually the statistical model including preequilibrium (PE) emission is applied. Whilst it is commonly taken for granted that a specific excitation function can be reproduced in the framework of these models, the simultaneous description of a large number (here 25) of reaction cross sections, involving many nuclides in common as intermediate and residual nuclei, with a consistent set of physically meaningful parameters and options still poses a challenge. Whereas the calculated total activation cross sections for nuclei are relatively insensitive to variations in the parameters governing the angular-momentum dependence, their distribution over ground and isomeric states is rather sensitive to all features influencing the spin distribution of the population of levels by particle emission and subsequent γ-ray cascades. In particular, attention should be given to the moments of inertia, assumptions regarding angular-momentum distribution in PE decay, spin and parity assignments of discrete levels, branching ratios of γ rays from discrete levels, and ratios of strengths of γ rays of different multipole types. Clearly, studies of isomeric ratios, both experimental and theoretical, for the same product nucleus formed in reaction systems involving different combinations of target, projectile, and ejectile promises to allow for separation of the influence of some of these components (cf. [6]). The present work describes a detailed and unified study in this direction. In Sec. II, the experiments are summarized, in Sec. III we describe the codes and parameters used in the reaction-model calculations. Their results are displayed and discussed in Sec. IV. In Sec. V, some conclusions are drawn from the present investigation.

II. EXPERIMENT

The experimental data used for comparison with the calculational results were based primarily on studies done at the Jülich cyclotron in the frame of optimization of the $^{94}Tc^m$ yield or as by-products of that work in the reactions $^{93}Nb+^3He$ [2], $^{92}Mo+\alpha$ [3], and $^{94}Mo+p$ [4,5]. Reactions whose excitation functions also resulted from the experiment described in Ref. [2], but have not been published so far are $^{93}Nb(^3He,x)^{93}Mo^m$, $^{93}Nb(^3He,x)^{92}Nb^m$, and $^{93}Nb(^3He,x)^{89}Zr^{m+g}$. We give here a short summary of those measurements.

Cross sections were measured by the well-known ''stacked-foil'' technique, commonly used at Jülich (cf. [2–4,7,8]). For studies on proton-induced reactions on enriched ^{94}Mo and α-particle-induced reactions on enriched ^{92}Mo, thin samples of $^{92,94}MoO_3$ were obtained by a sedimentation process and irradiations were done at low currents of 100–200 nA. The primary projectile energy used was 19.2 MeV in the case of protons and 27.1 MeV for α particles. The beam currents were determined via the monitor reactions $^{63}Cu(p,n)^{63}Zr$ and $^{nat}Ti(\alpha,xn)^{51}Cr$. The radioactivity of each investigated product was determined either nondestructively or radiochemically in combination with high-resolution γ-ray spectrometry. The results have been given in detail earlier (cf. [3,4]) and compared with the other published values [9–11].

In studies on ^3He-particle-induced reactions on ^{93}Nb, thin Nb foils (5 and 10 μm) were used as target material [2]. Irradiations were done at 200 nA using two primary ^3He-particle energies of 35.8 and 24.7 MeV. The beam current was measured directly using a Faraday cup as well as indirectly via the monitor reaction $^{nat}Ti(^3He,x)^{48}V$ (cf. [8]). The radioactivity of all the products was determined nondestructively using high-resolution γ-ray spectrometry. The results on the formation of $^{95}Tc^{m,g}$, $^{94}Tc^{m,g}$, and $^{93}Tc^{m,g}$ via $(^3He,xn)$ processes on ^{93}Nb have already been described [2] and compared with the literature data (cf. [12–14]). Some newer data, namely the production cross sections for $^{93}Mo^m$, $^{92}Nb^m$, and $^{89}Zr^{m+g}$, are now presented in Table I. Correctly speaking, what is termed as $^{89}Zr^{m+g}$ production cross section here comprises the ground-state production plus that fraction (93.77%) of the isomeric-state production which decays ($T_{1/2}=4.18$ min) to the ground state. The errors in cross sections include both random and systematic errors. The deviations in the particle energies are not errors; they describe the energy spread within each foil. Our data for the formation of $^{93}Mo^m$ are in agreement with the values of Flach [12] near the threshold of the reaction, but deviate considerably around the maximum of the excitation function. For the other two nuclides ($^{92}Nb^m$ and $^{89}Zr^{m+g}$) the data have not been measured previously.

The products $^{93}Mo^m$ ($T_{1/2}=6.9$ h), $^{92}Nb^m$ ($T_{1/2}=10.15$ d), and $^{89}Z^g$ ($T_{1/2}=78.4$ h) can be formed via various routes, e.g., $^{93}Nb(^3He,p2n+dn+t)^{93}Mo^m$, $^{93}Nb(^3He,2p2n+\alpha)^{92}Nb^m$, and $^{93}Nb(^3He,\alpha p2n+\alpha dn+\alpha t)^{89}Zr^{m+g}$, respectively. The thresholds and complex shapes of the excitation functions (see below) suggest the contribution of several processes.

The data were supplemented by cross sections retrieved from the literature for the reactions measured at Jülich, but also for reactions related to these either in immediate competition [e.g., $^{92}Mo(\alpha,p)^{95}Tc^m$] or by a subsequent emission step [e.g., $^{93}Nb(^3He,4n)^{92}Tc$], as well as for the $^{95}Mo(p,n)^{95}Tc$ reaction proceeding via the same intermediate system (^{96}Tc) as $^{93}Nb+^3He$. It was found difficult to set limits to including further reactions for which measurements exist, as many of the reactions for which there are data (e.g.,

TABLE I. Measured cross sections of $^{93}Nb(^3He,x)^{93}Mo^m$, $^{93}Nb(^3He,x)^{92}Nb^m$, and $^{93}Nb(^3He,x)^{89}Zr^{m+g}$ processes.

Incident energy (MeV)	Cross section (mb)	Cross section (mb)	Cross section (mb)
35.0±0.4	156.0±18.7	8.5±1.3	15.7±1.9
34.2±0.6	165.6±19.9	8.1±1.2	8.6±1.0
33.4±0.6		7.5±1.1	7.2±0.9
32.7±0.4	161.6±19.4	6.9±1.0	3.5±0.7
31.9±0.4	162.0±19.4	6.3±1.0	4.0±0.6
30.9±0.4	165.0±19.8	5.4±0.8	1.2±0.3
30.4±0.4	155.3±18.6		
30.1±0.4	165.0±19.8	5.1±0.8	
29.5±0.4	150.8±18.1	4.9±0.7	
28.4±0.2	143.0±17.1	4.2±0.6	
27.5±0.2	134.0±16.1		
26.6±0.2		3.7±0.6	
26.1±0.2	117.0±14.0		
25.6±0.2	110.0±13.2	3.9±0.6	
24.7±0.2		2.8±0.6	
24.3±0.2	107.0±12.8		
23.8±0.2	62.2±7.5		
23.5±0.2	73.6±8.8	3.1±0.6	
23.3±0.3	60.0±7.2		
23.2±0.3	62.0±7.4		
23.0±0.3	64.7±7.8		
22.7±0.3	61.0±7.3		
22.5±0.3	53.9±6.5	2.7±0.5	
22.2±0.3	60.0±7.2		
21.9±0.3	46.1±5.5		
21.7±0.3	45.0±5.4		
21.4±0.3	34.3±4.5	2.8±0.6	
21.1±0.3	39.0±7.0		
20.6±0.3	36.0±7.2	2.7±0.6	
20.0±0.3	13.6±2.7		
19.4±0.3	11.8±2.4		
19.1±0.3	18.0±3.6	2.4±0.5	
18.8±0.3	8.3±1.7	2.5±0.5	
18.5±0.3	12.0±2.4		
18.2±0.3	4.2±1.1		
17.9±0.3	7.6±1.9	2.3±0.5	
17.7±0.3	1.8±0.5	2.5±0.6	
17.0±0.3	1.4±0.7		
16.7±0.3	2.6±0.8		
16.4±0.2		2.0±0.4	
15.4±0.2		1.9±0.4	
14.7±0.2		1.6±0.4	
14.0±0.2		1.3±0.3	
13.3±0.2		1.0±0.3	
11.2±0.2		0.2±0.1	

$^{89}Y+^{3}He$ [12]) have some of the involved nuclides in common with the reactions considered here and could therefore be useful for parameter testing. But it is doubtful whether the enhanced parameter validation is worth the effort of taking the data base onto an unintelligible magnitude, when many of the nuclear-structure data for $Z=39-41$ have already been verified in previous works on neutron-induced reactions on $^{90,91}Zr$ [15], ^{92}Mo [16], and ^{93}Nb [17]. The reactions included in the data base, together with the energy ranges and authors of the various experiments, are compiled in Table II.

III. NUCLEAR REACTION-MODEL CALCULATIONS

The statistical model calculations were performed with the code STAPRE [18], which employs the Hauser-Feshbach formalism for equilibrium emission and the exciton model for PE emission.

For generating transmission coefficients, we used the spherical optical model as coded in the computer program ABACUS [19]. The optical potentials chosen for these calculations were those of Rapaport *et al.* [20] for neutrons, Mani *et al.* [21] for protons, Hinterberger *et al.* [22] for deuterons, Becchetti and Greenlees [23] for ^{3}H and ^{3}He, and Huizenga and Igo [24] for α particles. The α-particle transmission coefficients were reduced by 10% with respect to the original values to account for the overestimation of absorption cross sections by the Huizenga-Igo potential observed by us in various mass regions. A comparison of the absorption cross sections of α particles on ^{92}Nb computed with the optical potential of Huizenga and Igo [24] and the five-parameter optical potential of McFadden and Satchler [25], however, yielded close agreement; the above reduction is, therefore, quite arbitrary. Regarding the charged projectiles in the reactions considered, the definition ranges of the corresponding optical potentials with respect to mass number and energy should warrant their appropriateness in the case of α particles and protons. For ^{3}He, however, the data base on whose analysis the determination of the optical potential of Ref. [23] relied, contained cross-section data for target nuclei out of the mass range relevant here only at 25 and 29 MeV. When we noticed that in the calculation of excitation functions of ^{3}He-induced reactions on ^{93}Nb, the low-energy onsets came at too low energies, and the maxima of the $^{93}Nb(^{3}He,xn)^{95,94,93}Tc$ reactions were too high, we tried out a variation of the real depth, the depth W_V, radius r_I, and diffuseness a_I of the imaginary potential, and the Coulomb radius, aiming at a shift at the low-energy edge and a reduction at the plateau of the absorption cross section. The size of these variations was suggested by the scatter of these values used for optical-model analyses in the considered mass range according to the compilation of Perey and Perey [26]. The desired effect was achieved best with values $W_V=20$ (instead of 47) MeV and $a_I=0.77$ (instead of 0.88) fm, therefore, these values were adopted.

Many of the authors whose data are included in the present data base performed model calculations themselves for comparison with their measured excitation functions, and achieved agreement mostly within a factor 2. Among those for ^{3}He-induced reactions, the investigation by Bissem *et al.* [13] is the most instructive, in that it points out the importance of both conserving the neutron-proton asymmetry of the projectile in the creation of excitons during the equilibration process, and assuming a spin distribution of residual-nucleus states by PE emission different from that resulting from the equilibrium emission. We therefore adopted the treatment of neutron-proton asymmetry (''charge conservation''), formulated by Gadioli *et al.* [27] and present in the STAPRE code for nucleon-induced reactions, also for ^{3}He as projectile. Furthermore, we reactivated an option for distributing the PE portion of the nucleon production spectra over residual-nucleus angular momenta which Scobel [28] had suggested in the frame of the analysis by Bissem *et al.* [13] utilizing the code ALICE [29] for PE emission together with a Hauser-Feshbach-only version of STAPRE then in use at Hamburg University. This treatment relies on the assumption that the orbital angular momentum vector of the particle emitted in PE is parallel to that of the projectile, and hence related to the absolute value of the latter, or also to the compound-nucleus spin, by the square root of the ratio of projectile and ejectile energies owing to equality of impact parameters. The standard option used in STAPRE assumes the spin distribution in PE to be equal to that in equilibrium emission. The influence of these options on the isomeric ratios will be shown in Sec. IV.

Apart from ''charge conservation'' and spin distribution in PE decay as two options important with ^{3}He as an incoming particle, also the contribution of direct reactions to primary α-particle emission may play a role. When no specific direct-reaction model is coupled to the statistical model code, the PE model should at least allow for the emission of preformed α clusters. Therefore, the formulation of this effect by the Milano [30] group, which is commonly considered in STAPRE calculations of nucleon-induced reactions, was also taken over for ^{3}He-induced processes; a preformation factor of 0.11 was used.

For the energy dependence of the average effective matrix element for residual interactions, the exciton-number-dependent formulation of Kalbach [31] was adopted. The constant k in the matrix element was chosen to be 157 MeV^3. The Pauli correction in the intrinsic transition rates governing the random-walk description of the equilibration process and the energy shifts in the particle-hole state densities accounting for pairing are given elsewhere [18]. The initial particle and hole numbers used for the various projectiles were (2,1) for protons, (4,1) for ^{3}He, and (4,0) for α particles.

At the equilibrium stage, the main ingredients are discrete-level data, including branching ratios of γ transitions between the levels, and level-density parameters. Nuclear-structure data libraries from which the STAPRE inputs are constructed automatically were set up in this mass range in the context of studies described in Refs. [15–17], and were updated and extended now on the basis of the Nuclear Data Sheets [32] and the compilation by Dilg *et al.* [33] of parameters for the back-shifted Fermi-gas model with full and half rigid-body values for the moments of inertia I_{eff}. The numbers of levels, the energies of the highest-lying levels, and the level-density parameters ($I_{\mathrm{eff}}/I_{\mathrm{rigid}}=1$) used for the involved nuclides are compiled in Table III.

Regarding γ-ray transmission coefficients, the strength functions for $E1$ radiation were derived from the photoab-

TABLE II. Experimental data underlying the theoretical study.

Quantity	Energy range (MeV) to (MeV)	Reference
^{93}Nb(^{3}He,n)^{95}Tc^{m,g}, exc. fct.	10.4–35.0	Faßbender *et al.* 1994 [2]
	8.9–27.3	Bissem *et al.* 1980 [13]
^{93}Nb(^{3}He,n)^{93}Tc^{m+g}, exc. fct.	12.8–42.8	Bissem *et al.* 1980 [13]
^{93}Nb(^{3}He,n)^{95}Tc, isomeric ratio	11.2–35.0	Faßbender *et al.* 1994 [2]
	8.9–23.7	Bissem *et al.* 1980 [13]
^{93}Nb(^{3}He,2n)^{94}Tc^{m,g}, exc. fct.	8.6–35.0	Faßbender *et al.* 1994 [2]
	14.0–35.1	Auler *et al.* 1981 [14]
	11.2–42.8	Bissem *et al.* 1980 [13]
	11.6–42.9	Flach 1976 [12]
^{93}Nb(^{3}He,2n)^{94}Tc isomeric ratio	8.6–35.0	Faßbender *et al.* 1994 [2]
	14.0–35.1	Auler *et al.* 1981 [14]
	11.2–42.8	Bissem *et al.* 1980 [13]
	11.6–42.9	Flach 1976 [12]
^{93}Nb(^{3}He,3n)^{93}Tc^{m,g} exc. fct.	15.9–35.0	Faßbender *et al.* 1994 [2]
	16.4–35.1	Auler *et al.* 1981 [14]
	15.8–42.8	Bissem *et al.* 1980 [13]
	15.0–42.9	Flach 1976 [12]
^{93}Nb(^{3}He,3n)^{93}Tc, isomeric ratio	16.1–35.0	Faßbender *et al.* 1994 [2]
	16.4–35.1	Auler *et al.* 1981 [14]
	15.8–42.8	Bissem *et al.* 1980 [13]
	17.6–42.9	Flach 1976 [12]
^{93}Nb(^{3}He,4n)^{92}Tc, exc. fct.	31.6–42.8	Bissem *et al.* 1980 [13]
	28.6–39.7	Flach 1976 [12]
^{93}Nb(^{3}He,x)^{93}Mo^{m}, exc. fct.	16.7–35.0	Present work
	15.0–42.9	Flach 1976 [12]
^{93}Nb(^{3}He,x)^{92}Nb^{m}, exc. fct.	9.5–35.0	Present work
^{93}Nb(^{3}He,x)^{89}Zr^{m+g}, exc. fct.	30.9–35.0	Present work
^{92}Mo(α,n)^{95}Ru, exc. fct.	11.8–26.8	Denzler *et al.* 1995 [4]
	12.0–30.0	Graf and Münzel 1974 [9]
	9.4–27.7	Esterlund and Pate [10]
^{92}Mo(α,2n)^{94}Ru, exc. fct.	18.8–26.8	Denzler *et al.* 1995 [4]
	19.0–41.0	Graf and Münzel 1974 [9]
^{92}Mo(α,p)^{95}Tc^{m}, exc. fct.	13.0–31.5	Graf and Münzel 1974 [9]
	10.0–29.0	Esterlund and Pate 1965 [10]
^{92}Mo(α,p)^{95}Tc^{g}, exc. fct.	18.1–26.8	Denzler *et al.* 1995 [4]
	12.0–27.0	Graf and Münzel 1974 [9]
	12.0–19.9	Esterlund and Pate [10]
^{92}Mo(α,x)^{94}Tc^{m,g}, exc. fct.	17.7–26.8	Denzler *et al.* 1995 [4]
	18.0–42.0	Graf and Münzel 1974 [9]
^{92}Mo(α,x)^{94}Tc, isomeric ratio	18.5–26.8	Denzler *et al.* 1995 [4]
	20.0–37.0	Graf and Münzel 1974 [9]
^{92}Mo(α,x)^{93}Tc^{m,g}, exc. fct.	26.1–55.0	Graf and Münzel 1974 [9]
^{92}Mo(α,x)^{93}Tc, isomeric ratio	33.0–55.0	Graf and Münzel 1974 [9]
^{94}Mo(p,n)^{94}Tc^{m,g}, exc. fct.	6.1–18.4	Rösch and Qaim 1993 [4]
	7.7–18.3	Levkovskij 1991 [37]
	5.5–9.0	Skakun *et al.* 1987 [11]
^{94}Mo(p,n)^{94}Tc, isomeric ratio	6.1–18.4	Rösch and Qaim 1993 [4]
	7.7–18.3	Levkovskij 1991 [37]
	6.0–9.0	Skakun *et al.* 1987 [11]
^{94}Mo(p,2n)^{93}Tc^{m,g}, exc. fct.	14.0–18.4	Rösch and Qaim 1993 [4]
	13.8–29.5	Levkovskij 1991 [37]
^{94}Mo(p,2n)^{93}Tc, isomeric ratio	14.0–18.4	Rösch and Qaim 1993 [4]
	14.8–29.5	Levkovskij 1991 [37]
^{95}Mo(p,n)^{95}Tc^{m,g}, exc. fct.	4.8–28.0	Izumo *et al.* 1991 [38]
	4.0–9.0	Skakun *et al.* 1987 [11]
^{95}Mo(p,n)^{95}Tc, isomeric ratio	4.8–28.0	Izumo *et al.* 1991 [38]
	4.0–9.0	Skakun *et al.* 1987 [11]

TABLE III. Discrete-level and level-density information ($I_{\text{eff}} = I_{\text{rigid}}$).

Nuclide	No. of levels	Energy of highest level (MeV)	a parameter (MeV^{-1})	Δ (MeV)
^{96}Ru	13	2.588	12.00	0.60
^{95}Ru	18	2.294	10.86	0.10
^{94}Ru	12	3.255	10.34	1.23
^{93}Ru	7	2.279	12.40	0.50
^{96}Tc	48	0.828	13.20	−1.39
^{95}Tc	49	2.189	11.50	−0.35
^{94}Tc	26	1.447	11.00	−0.76
^{93}Tc	27	2.631	10.30	−0.10
^{92}Tc	23	1.800	11.00	−1.00
^{95}Mo	24	1.698	11.27	−0.63
^{94}Mo	20	2.872	11.34	0.58
^{93}Mo	43	2.822	11.36	0.00
^{92}Mo	11	3.091	10.27	1.45
^{92}Nb	34	1.738	11.50	−0.55
^{89}Zr	10	1.944	10.26	0.07

sorption cross section, using the values $E_0 = 75A^{-1/3}$ MeV, $\Gamma = 5.5$ MeV for resonance energy and width. Also for $M1$ radiation, the strength functions were derived from an absorption cross section of Lorentzian shape with global parameters for resonance energy, width and peak cross section ($E_0 = 41A^{-1/3}$ MeV, $\Gamma = 4.0$ MeV). For both multipole types, the values of the peak cross sections were overridden by normalization factors applied to adjust the strength functions for these multipole types at the neutron binding energy to the values given by Kopecky and Uhl [34]. Variations of the absolute $E1$ strength and $M1/E1$ ratio were found to have little influence on the isomeric ratios. For the other multipole types considered, i.e., $E2$, $M2$, $E3$, and $M3$, the strength functions were computed from the Weisskopf model and normalized relative to the $E1$ strength function at the neutron binding energy according to the Weisskopf estimate.

IV. RESULTS AND DISCUSSION

A. ^{3}He-induced reactions on ^{93}Nb

The experimental data, together with the results of the model calculations, for the excitation functions for ground (g) and, if existent, isomeric (m) states for the ^{93}Nb(^{3}He,xn)^{95,94,93,92}Tc ($x = 1,...,4$) reactions and, where applicable, the isomeric cross-section ratios are displayed in Figs. 1–4. The isomeric cross-section ratios $\sigma^m/(\sigma^m+\sigma^g)$ of these and all further reactions were assigned uncertainties calculated considering the correlation of uncertainties of σ^m and σ^g for all Jülich data, but assuming uncorrelated uncertainties of σ^m and σ^g for all other data sets owing to lack of corresponding information. For ^{93}Nb(^{3}He,n)^{95}Tc, the summed activation cross section σ^{m+g} is given in a separate plot, as the EXFOR entry consisting of the work of Bissem *et al.* [13] contains these values without splitting into σ^m and σ^g in addition to the data for σ^m and σ^g displayed in Figs. 1(a) and 1(b); the two sets of data stem from independent measurements at Bonn and Hamburg. All figures contain the results of calculations with Hauser-Feshbach (HF) weights as well as the Scobel assumption for the spin distribution of particles emitted at the PE stage, both used together with the rigid-body moments of inertia ($\eta = I_{\text{eff}}/I_{\text{rigid}} = 1$). As a further option, we display calculations with the weights in the PE spin distribution taken from equilibrium emission, but utilizing $\eta = 0.5$ in the HF formalism. The level-density pa-

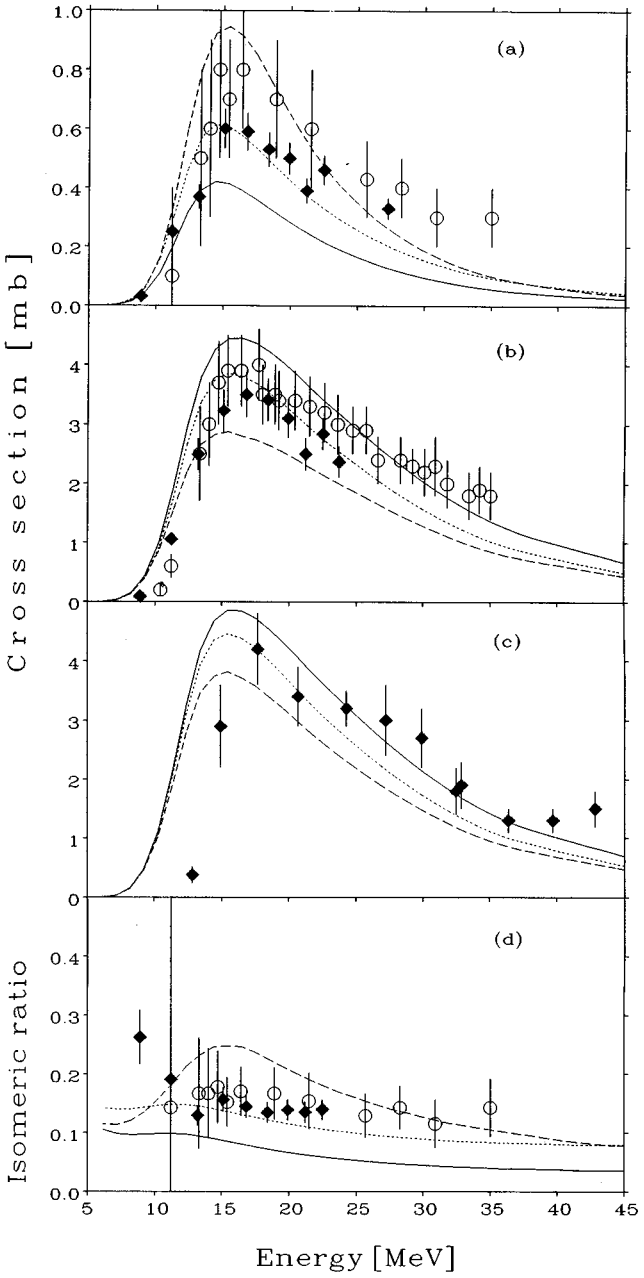

FIG. 1. (a) Cross sections for the ^{93}Nb(^{3}He,n)^{95}Tc^m reaction. (b) Cross sections for the ^{93}Nb(^{3}He,n)^{95}Tc^g reaction. (c) Cross sections for the ^{93}Nb(^{3}He,n)^{95}Tc^{m+g} reaction. (d) Isomeric ratio for the ^{93}Nb(^{3}He,n)^{95}Tc reaction. Open circles, Faßbender *et al.* [2]; full diamonds, Bissem *et al.* [13]; solid line, calculation with back-shifted Fermi-gas level densities ($I_{\text{eff}} = I_{\text{rigid}}$) and Hauser-Feshbach-weighted spin distribution in PE decay; dashed line, calculation with back-shifted Fermi-gas level densities ($I_{\text{eff}} = I_{\text{rigid}}$) and spin distribution in PE decay according to Scobel; dotted line, calculation with back-shifted Fermi-gas level densities ($I_{\text{eff}} = 0.5 I_{\text{rigid}}$) and HF-weighted spin distribution in PE decay.

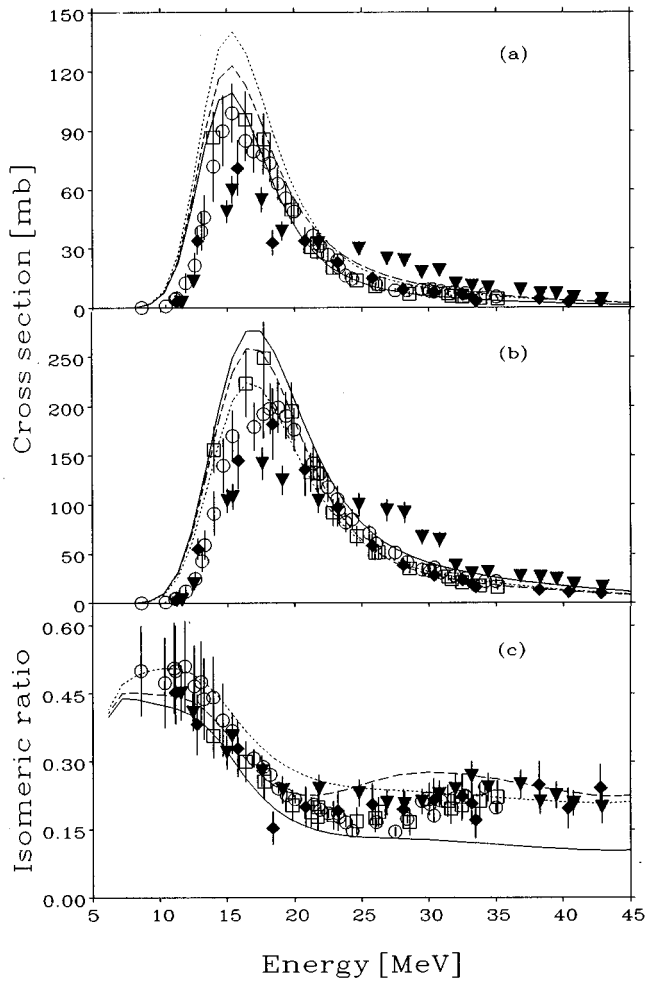

FIG. 2. (a) Cross sections for the ^{93}Nb(^{3}He,2n)^{94}Tc^{m} reaction. (b) Cross sections for the ^{93}Nb(^{3}He,2n)^{94}Tc^{g} reaction. (c) Isomeric ratio for the ^{93}Nb(^{3}He,2n)^{94}Tc reaction. Open circles, Faßbender *et al.* [2]; open squares, Auler *et al.* [14]; full diamonds, Bissem *et al.* [13]; full triangles down, Flach [12], explanation of lines as in Fig. 1.

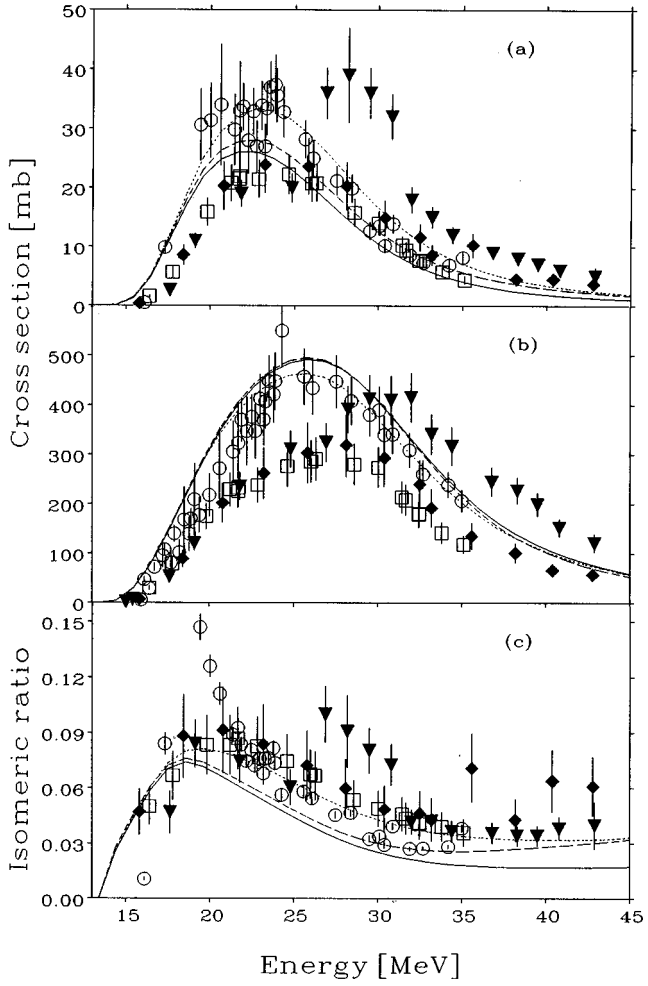

FIG. 3. (a) Cross sections for the ^{93}Nb(^{3}He,3n)^{93}Tc^{m} reaction. (b) Cross sections for the ^{93}Nb(^{3}He,3n)^{93}Tc^{g} reaction. (c) Isomeric ratio for the ^{93}Nb(^{3}He,3n)^{93}Tc reaction. Explanation of symbols and lines as in Fig. 2.

rameters for the reduced moments of inertia differ from those for the rigid-body values by reductions by about one unit in a and by 0.0–0.2 MeV in Δ.

In the ^{93}Nb(^{3}He,n)^{95}Tc reaction, the formation of both g and m states [Figs. 1(a) and 1(b)] would be well reproduced by a curve intermediate between the above two assumptions (HF weights versus Scobel) on spin dependence of the PE contribution computed with $\eta=1$. In fact, this result is achieved with HF weights and $\eta=0.5$. In the (^{3}He,2n) reaction, there is a smaller, but still appreciable shift of cross section from the high-spin (g) to the low-spin (m) state in ^{94}Tc when changing from the standard to the Scobel formulation, and a further increase of this effect by use of $\eta=0.5$. The ground- as well as the isomeric-state production [Fig. 2(a)] is somewhat overestimated with HF weights and $\eta=1$; therefore, the isomeric ratio [Fig. 2(c)] is reasonably reproduced, with the two $\eta=1$ curves enveloping the measured values above 20 MeV. The results with HF weights and $\eta=0.5$ are worse than the other two below 25 MeV, but better above this energy. In the (^{3}He,3n) reaction there is no substantial difference between the two curves with $\eta=1$. The measured m-state activation in ^{93}Tc [Fig. 3(a)] is underestimated by the calculation beyond 25 MeV and so is the isomeric cross-section ratio [Fig. 3(c)] in the entire energy range. These shortcomings are alleviated by using $\eta=0.5$. It appears that the Jülich cross-section data for both m and g states [2] in the energy range 20–25 MeV and also the Flach m and g data [12] for incident energies above about 27 MeV differ systematically from the rest of the data. Consequently, the experimental isomeric ratios are somewhat more consistent than the m- and g-state cross sections. Finally, the theoretical ^{92}Tc-production curve (Fig. 4) is lower compared to the measured data by about 30%.

The slight overshoot of calculation versus experiment in ^{94,93}Tc production together with the underprediction of ^{92}Tc formation may suggest that the calculated particle production spectra in the first few emission steps are too hard. Consequently, the (^{3}He,2n) and (^{3}He,3n) cross sections are overestimated at the expense of the (^{3}He,4n) cross section. The means of shifting the neutron production from higher to lower neutron energies in the calculated spectra are a reduction of PE emission or a selective increase of level densities

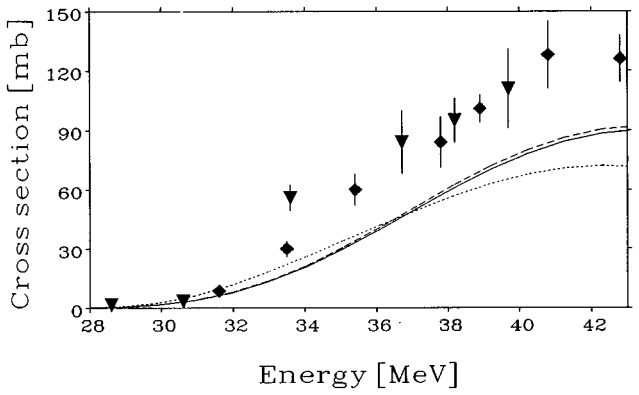

FIG. 4. Cross sections for the ^{93}Nb(^{3}He,4n)^{92}Tc reaction. Full diamonds, Bissem *et al.* [13]; full triangles down, Flach [12], explanation of lines as in Fig. 1.

at high excitation energies. As regards the former, we experienced this effect when comparing (3,0) with (4,1) for the initial particle and hole number in the equilibration process of the composite system, but a further increase of these numbers is not plausible for ^{3}He as a projectile. Also, the inclusion of charge conservation in the original Milano formulation [27] caused an increase in the PE fraction (i.e., percentage of the absorption cross section which is depleted by PE particle emission) and was, therefore, modified by multiplying the factor $(n\pm1)/n$ (with n the exciton number) with the combinatorial probability for formation of the ejectile from its nucleons. In this way, we also achieved reasonable consistency between the PE fractions in the reactions induced by different types of projectiles. The other approach, namely a variation in the shape of the equilibrium portion of the neutron production spectra, may be attempted by using level densities with shell corrections fading out at high excitation energies [35]. This option was not available.

In Fig. 5, we present the experimental and theoretical results on the formation of ^{93}Mo^{m}, ^{92}Nb^{m}, and ^{89}Zr^{m+g} from ^{93}Nb+^{3}He. Obviously, the production of ^{93}Mo requires the emission of one proton and two neutrons in any order (including $d+n$ and t). The production of ^{92}Nb, on the other hand, involves the emission of two protons and two neutrons either as a sequence of single nucleons or of an α particle or a deuteron plus two nucleons, and that of ^{89}Zr the emission of 3 protons and 4 neutrons, including clusters like α, t, or d. The limitations of the STAPRE version utilized, namely to consider no ejectiles heavier than ^{4}He (i.e., the contribution of ^{7}Li emission to the ^{89}Zr production was neglected) and no more than 6 sequential emissions, were retained. The calculated ^{89}Zr^{m} cross sections were reduced by 6.23% to account for the decay via electron capture and positron emission (thereby not contributing to the formation of the ground state). As can be seen from the figures, the activation of ^{93}Mo^{m} and ^{89}Zr^{m+g} is described quite nicely, as all the major contributing reaction paths with their relevant reaction mechanisms are considered. The contribution of the (^{3}He,t) charge-exchange reaction in the formation of ^{93}Mo^{m}, which was not considered here, appears to be relatively small. In the case of ^{92}Nb^{m} the contribution of (^{3}He,α) pickup is missing. We roughly estimated this contribution to the

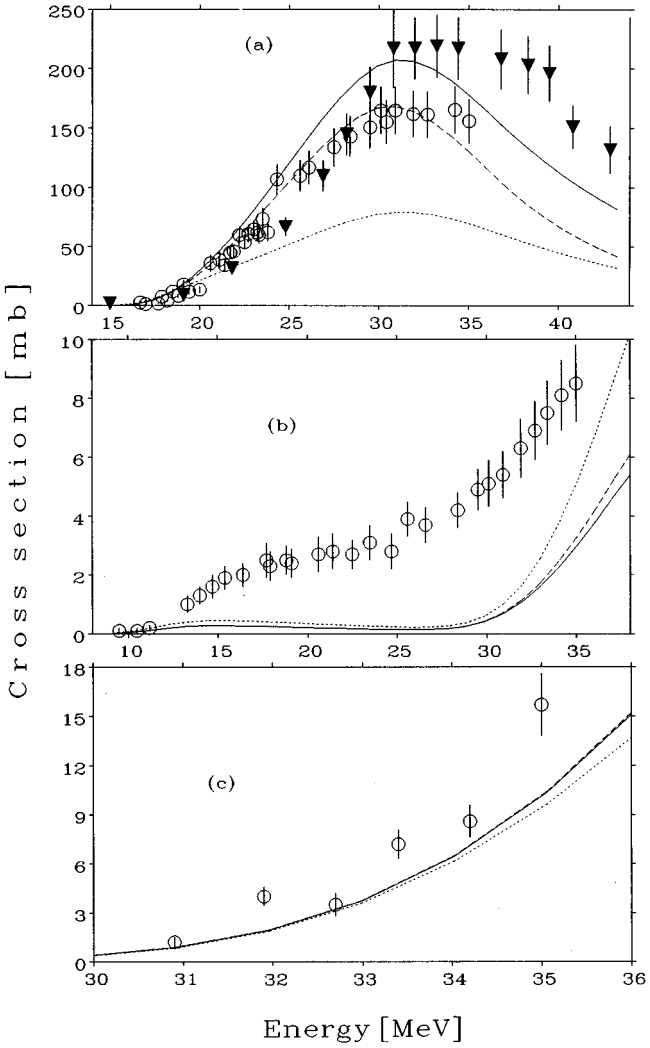

FIG. 5. (a) Cross sections for the ^{93}Nb(^{3}He,x)^{93}Mo^{m} reaction. (b) Cross sections for the ^{93}Nb(^{3}He,x)^{92}Nb^{m} reaction. (c) Cross sections for the ^{93}Nb(^{3}He,x)^{89}Zr^{m+g} reaction. Open circles, present work; full triangles down, Flach [12], explanation of lines as in Fig. 1.

m-state activation cross section from the measured maximum angle-differential cross sections [36] for the population of levels of ^{92}Nb in the neutron-pickup reaction ^{93}Nb(^{3}He,α) at 19.5 MeV incident ^{3}He energy. This estimate amounts to 1 mb, well suited to make up for the difference between measured and calculated cross sections in Fig. 5.

B. α-particle-induced reactions on ^{92}Mo

Figures 6–9 depict the results for α-particle-induced reactions on ^{92}Mo. In all figures the same symbol (open circle) was used for the Jülich data, even though they were published in different papers. Excitation functions computed on the Scobel assumptions are not displayed as separate curves as they do not show any significant difference from those obtained with HF weights. As seen in Fig. 6, for ^{92}Mo(α,xn)^{95,94}Ru (x=1,2), the excitation functions calculated with η=0.5 and 1 are somewhat high, with large scatter in the experimental data, too. For ^{92}Mo(α,p)^{95}Tc^{m} [Fig.

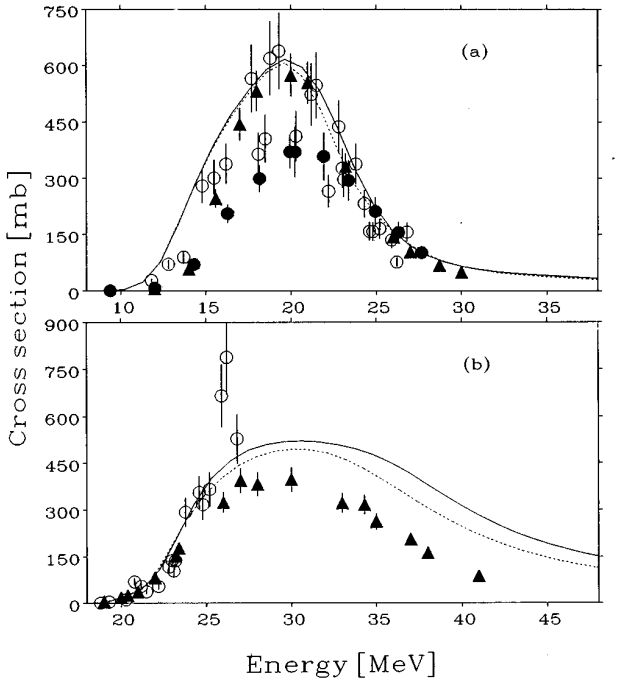

FIG. 6. (a) Cross sections for the ^{92}Mo(α,n)^{95}Ru reaction. (b) Cross sections for the ^{92}Mo(α,$2n$)^{94}Ru reaction. Explanation of symbols and lines as in Fig. 6.

7(a)], the calculations show a shift of about 2 MeV to the lower energy with respect to the experimental data, but the magnitude is of proper size. The compiler of the EXFOR entry (B0040.007) points out a problem in the value used by Graf

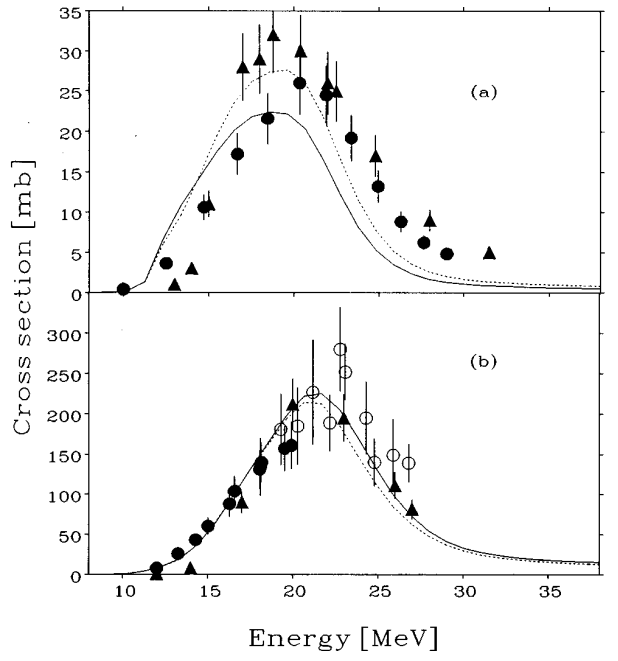

FIG. 7. (a) Cross sections for the ^{92}Mo(α,p)^{95}Tc^{m} reaction. (b) Cross sections for the ^{92}Mo(α,p)^{95}Tc^{g} reaction. Open circles, Denzler *et al.* [3]; full triangles up, Graf and Münzel [9]; full circles, Esterlund and Pate [10], explanation of lines as in Fig. 1.

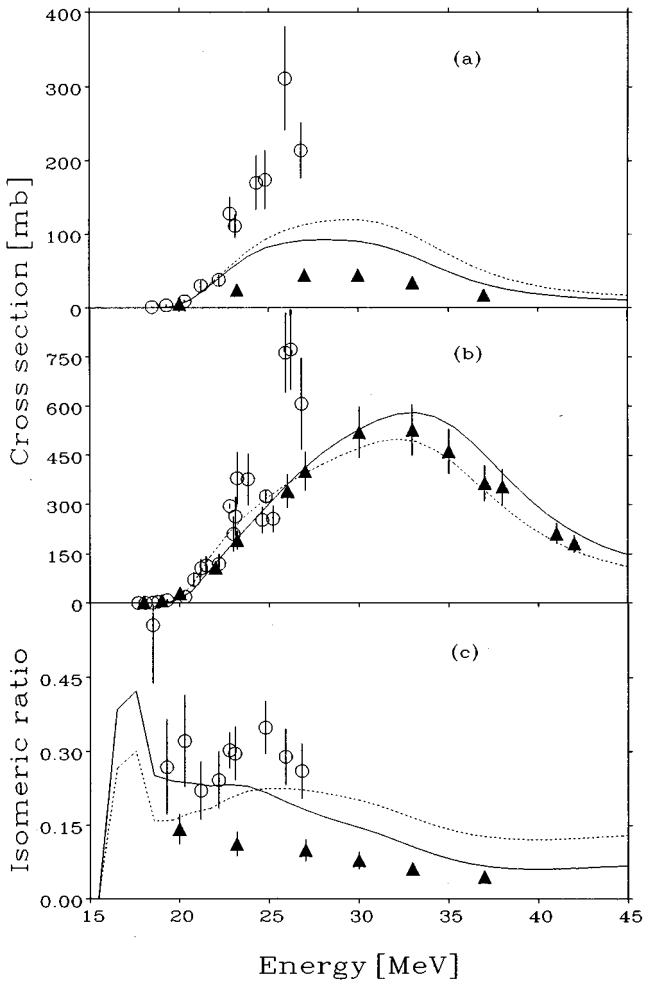

FIG. 8. (a) Cross section for the ^{92}Mo(α,x)^{94}Tc^{m} reaction. (b) Cross section for the ^{92}Mo(α,x)^{94}Tc^{g} reaction. (c) Isomeric ratio for the ^{92}Mo(α,x)^{94}Tc reaction. Open circles, Denzler *et al.* [3]; full triangles up, Graf and Münzel [9], explanation of lines as in Fig. 1.

and Münzel [9] for the intensity of the 204-keV γ line of ^{95}Tc^{m}. Correcting this value would increase the ^{92}Mo(α,p)^{95}Tc^{m} cross sections by 30%. This would neither remove their deviation from the cross-section values of Esterlund and Pate [10] nor from the model calculation. For ^{92}Mo(α,p)^{95}Tc^{g} [Fig. 7(b)], the consistency of the different data sets and their description by theory is good. No isomeric cross-section ratio is defined by the measured g- and m-state cross sections, as they were taken at different incident α energies. In Figs. 8(a) and 8(b), we show the activation cross sections for the m and g states in ^{92}Mo(α,x)^{94}Tc. In both reactions, there is a deviation of the Jülich data around 26 MeV from the rest of the data set, as is the case in ^{92}Mo(α,$2n$)^{94}Ru. For ^{92}Mo(α,x)^{94}Tc^{m} ($x=p+n,n+p,d$), the two sets of measured cross sections are very discrepant. The major difficulty lies in the subtraction of the contribution of the

$$^{94}\mathrm{Ru}\xrightarrow{EC}{}^{94}\mathrm{Tc}^{m}$$

process at the time of measurement. The model calculations

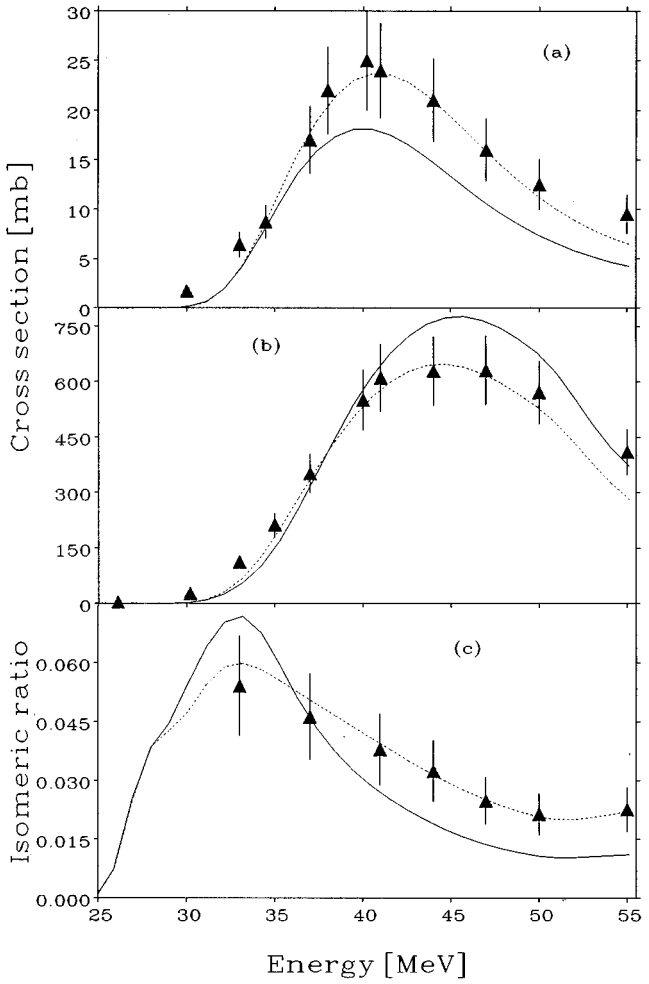

FIG. 9. (a) Cross sections for the ^{92}Mo(α,x)^{93}Tc^{m} reaction. (b) Cross sections for the ^{92}Mo(α,x)^{93}Tc^{g} reaction. (c) Isomeric ratio for the ^{92}Mo(α,x)^{93}Tc reaction. Full triangles up, Graf and Münzel [9], explanation of lines as in Fig. 1.

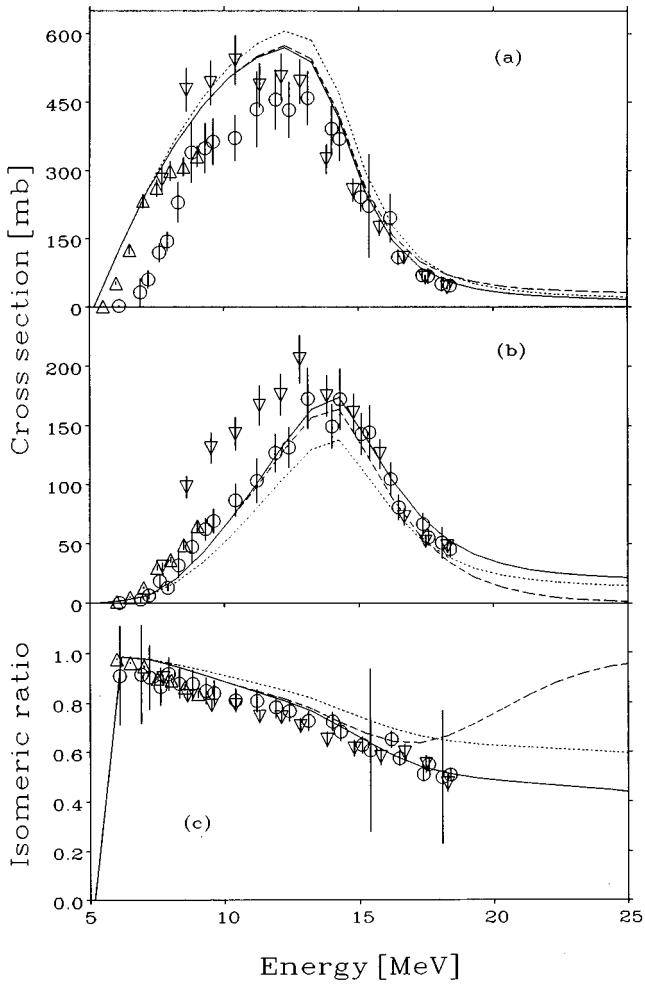

FIG. 10. (a) Cross sections for the ^{94}Mo(p,n)^{94}Tc^{m} reaction. (b) Cross sections for the ^{94}Mo(p,n)^{94}Tc^{g} reaction. (c) Isomeric ratio for the ^{94}Mo(p,n)^{94}Tc reaction. Open circles, Rösch and Qaim [4]; open triangles down, Levkovskij [37]; open triangles up, Skakun [11], explanation of lines as in Fig. 1.

given here do not allow for a decision between the two sets of experimental data. The ^{92}Mo(α,x)^{94}Tc^{g} data are more consistent and described well by the theory. In this case there is no contribution from the decay of ^{94}Ru. The problems of the m-state excitation function are reflected in a discrepancy between the measured and calculated isomeric cross-section ratio [Fig. 8(c)]. Nonetheless, the results of model calculations are closer to the Jülich data than the other data. For the nucleus resulting from the emission of one further neutron, namely ^{93}Tc, we took the data from the literature [9] in order to check the reproduction of the formation of ground and isomeric states and the isomeric ratio. While the $\eta=1$ calculation for ^{92}Mo(α,x)^{93}Tc^{m} [Fig. 9(a)] is below the measured points for energies above 35 MeV, the calculated ^{92}Mo(α,x)^{93}Tc^{g} cross sections [Fig. 9(b)] are larger than the measured values; the experimental isomeric ratio [Fig. 9(c)] is, therefore, underestimated by the calculated result beyond 35 MeV energy. Here, the shortcomings in the description of the ^{93}Tc^{m,g} production are overcome by use of the reduced moments of inertia. There is no clear evidence whether the reduction of the α-particle transmission coefficients, which is directly passed on to the activation cross sections via the absorption cross sections, is the right choice: five out of eight α-induced excitation functions on ^{92}Mo are improved by this modification.

C. Proton-induced reactions on ^{94,95}Mo

The excitation functions of proton-induced reactions on ^{94,95}Mo are displayed in Figs. 10–12. The calculated $\eta=1$ excitation functions for the ^{94}Mo(p,n)^{94}Tc^{m,g} reactions [Figs. 10(a) and 10(b)] are in good agreement with the experimental ones, apart from a slight overestimate of the m-state production, which is reflected in the isomeric ratio [Fig. 10(c)]. The isomeric ratio computed on the Scobel assumption increases strongly above 17 MeV incident energy; the experimental data confirm the continued decrease of the HF-weighted PE spin distribution. The effect of $\eta=0.5$ on all the three quantities displayed is disadvantageous. The Levkovskij data [37] show considerable deviations for ^{94}Mo(p,n)^{94}Tc^{m} in the range 8.6–10.4 MeV, for ^{94}Mo(p,n)^{94}Tc^{g} between 8.6 and 12.8 MeV from the rest of this very data set as well as the other two measurements

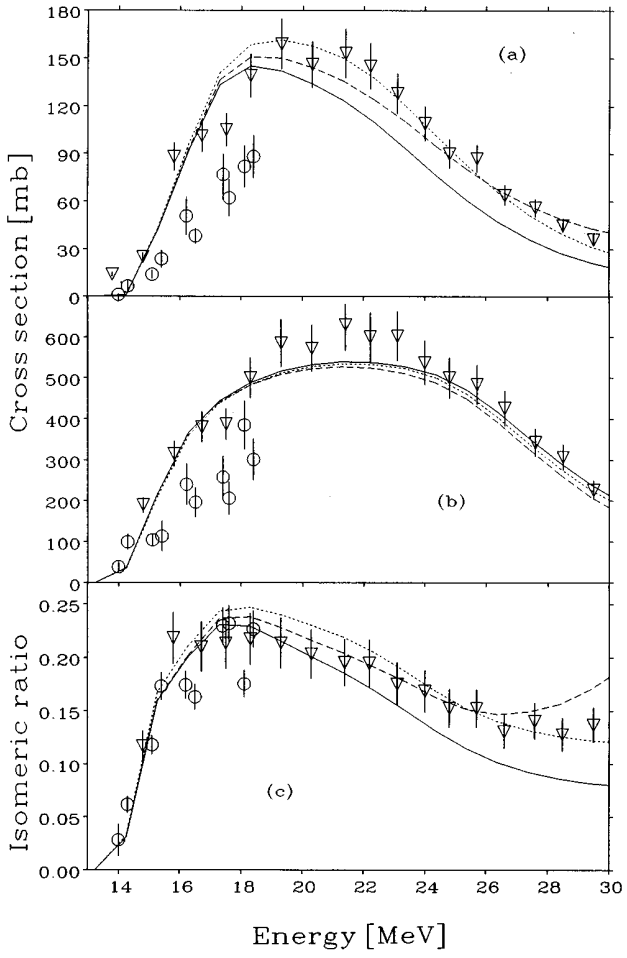

FIG. 11. (a) Cross sections for the ^{94}Mo(p,2n)^{93}Tc^{m} reaction. (b) Cross sections for the ^{94}Mo(p,2n)^{93}Tc^{g} reaction. (c) Isomeric ratio for the ^{94}Mo(p,2n)^{93}Tc reaction. Open circles, Rösch and Qaim [4]; open triangles down, Levkovskij [37], explanation of lines as in Fig. 1.

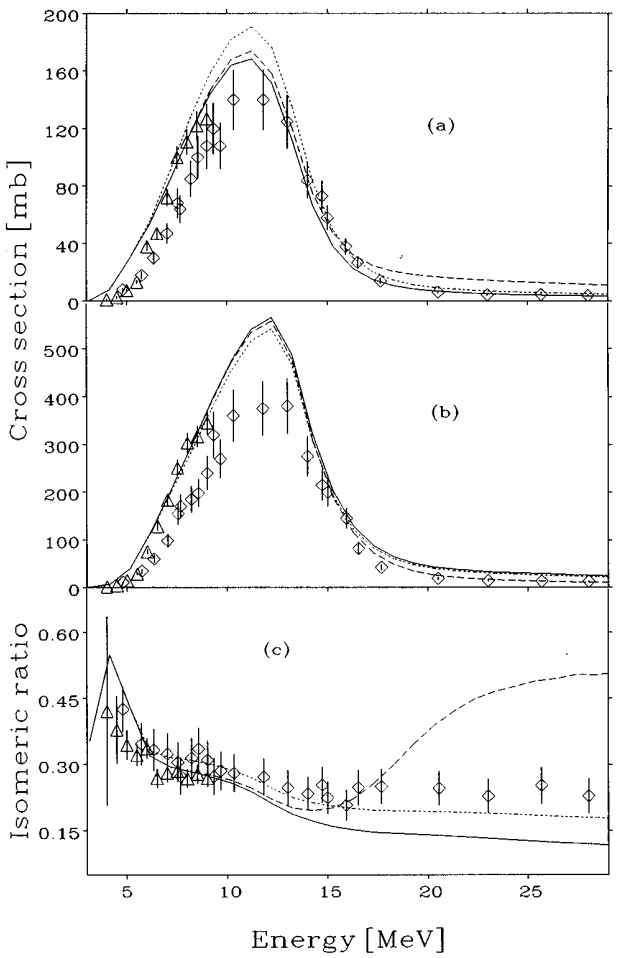

FIG. 12. (a) Cross sections for the ^{95}Mo(p,n)^{95}Tc^{m} reaction. (b) Cross sections for the ^{95}Mo(p,n)^{95}Tc^{g} reaction. (c) Isomeric ratio for the ^{95}Mo(p,n)^{95}Tc reaction. Open diamonds, Izumo *et al.* [38]; open triangles up, Skakun [11], explanation of lines as in Fig. 1.

[4,38]. In the case of ^{94}Mo(p,2n)^{93}Tc^{m,g} the Levkovskij data set [37] is more consistent in itself and with the calculations [Figs. 11(a) and 11(b)], but the Jülich data [4], given between 14.0 and 18.4 MeV, are lower. The isomeric cross-section ratios up to 16 MeV are, however, more consistent. The effects of both the Scobel option and of $\eta=0.5$ are favorable to the reproduction of the measured values of the m-state [Fig. 11(a)] and hence isomeric ratios above about 18 MeV [see Fig. 11(c)].

Finally, the ^{95}Mo(p,n)^{95}Tc^{m,g} reaction cross sections as measured by Izumo *et al.* [38] and Skakun *et al.* [11] are compared with our calculations in Figs. 12(a) and 12(b) and appear to be somewhat overestimated by these. As for the isomeric ratio [Fig. 12(c)] all three options regarding the PE spin distribution yield a good description up to 15 MeV; at higher incident energies, the standard weighting with $\eta=0.5$ is clearly superior over $\eta=1$, and the Scobel option gives an increase which deviates strongly from the experimental points.

V. CONCLUSIONS

The investigation described here demonstrates that a large body of experimental excitation functions of charged-particle-induced reactions proceeding via the composite systems ^{95,96}Tc and ^{96}Ru, together with the isomeric cross-section ratios involved, can be described properly within the framework of phenomenological reaction models. For this purpose, only minor adjustments were made on the parameters obtained from independent experimental information (like level-density parameters) or from probate prescriptions (like PE parameters), as would be prepared for a ''Reference Input Parameter Library'' in the sense of the corresponding IAEA Coordinated Research Programme.

Clearly, in calculating the isomeric cross sections, particular attention has to be paid to the description of the angular-momentum dependence of the population of all intermediate and residual nuclei. The present work shows that when the PE cross sections are distributed over the spins of the residual nucleus according to their population in the HF formalism under usage of the rigid-body moments of inertia, the proportion of high- and low-spin isomer production is not reproduced properly in numerous cases. An improvement is achieved when favoring the population of residual-nucleus states of low spin. This is accomplished by enhancing higher orbital angular momenta in PE emission which affects mainly the population of the nuclide resulting from the first emission step, or by reducing the effective moments of iner-

tia with respect to the rigid-body values in the entire formalism, which acts in all nuclides involved in the emission sequence. While it may appear desirable to change the description of angular-momentum dependence in PE decay from the application of the HF weights, the present investigation shows that with very few exceptions the use of this option together with decreased moments of inertia yields an even more convincing improvement in the description of the experimental excitation functions by the model calculations. Here, a value of 0.5 for $I_{\rm eff}/I_{\rm rigid}$ was used; a value of 0.7 was obtained in Ref. [10]; 0.75 was found appropriate for this quantity in a study involving a neighboring mass region, namely ^{103}Rh$+n$ [39]. Combining the modified PE treatment, i.e., preferring population of low-spin residual states, with the reduced moments of inertia would multiply this effect and makes the fits to the isomeric-state cross sections worse.

It is worthwhile to deliberate whether the consideration of isospin would change the results significantly. An upper limit of this effect may be estimated by forcing that fraction of the absorption cross sections that leads to formation of $T^{>}$ states in the reaction systems ^{93}Nb$+^{3}$He and ^{94,95}Mo$+p$ into the proton channel. It appears this would not generally improve the fits, as there is not a systematic deficiency of this magnitude ($\approx$10%) in the calculated neutron emission cross sections.

It has to be emphasized that in all cases under consideration, the trends in the isomeric cross-section ratios are reproduced correctly by the calculations even where their magnitude is not predicted as nicely.

For an improved experimental knowledge of the reactions under investigation, as well as for a fairer judgment of the quality of their theoretical description, however, it would be useful to resolve the discrepancies existing among the various data sets. According to our experience [40] with neutron-induced reactions, such a clarification is in many cases not possible merely on the grounds of how the experiment is documented in the publication. Direct communication with the experimenters is required, which in the context of the present study would be difficult as some of the measurement were done over 30 years ago.

One example for such unclear effects is the following: Flach's ^{93}Nb(^{3}He,xn)^{94,93}Tc^{m,g} ($x=2,3$) data [12] undergo a transition from a relatively low data set to a very high data set at about the energy where the change from ^{65}Cu(^{3}He,$2n$)^{66}Ga to ^{27}Al(^{3}He,$\alpha 2p$)^{24}Na as monitor reaction occurs. As he even revised the ^{27}Al(^{3}He,$\alpha 2p$)^{24}Na cross sections to achieve consistency between the integrated currents obtained with the two monitor reactions in the energy region where both are available, it is not clear whether the rise in the ^{93}Nb(^{3}He,xn)^{94,93}Tc ($x=2,3$) cross sections is correlated with the change in the monitor reaction. A similar phenomenon occurs in the ^{93}Nb(^{3}He,x)^{93}Mo^{m} excitation function at 30 MeV.

The optical potentials given by Becchetti and Greenlees for ^{3}He and ^{3}H, even though widely used, lack experimental confirmation towards low energies. Slight parameter modifications of the ^{3}He potential improved the description of the shape of the ^{3}He-induced excitation function at the low-energy edge. Especially in view of constructing reference input parameter libraries for reaction-model calculations, it would be desirable to have optical potentials which are also global with respect to mass number but are better validated throughout the energy range required.

ACKNOWLEDGMENTS

Thanks are due to the crew of the Jülich compact cyclotron (CV 28) for performing the irradiations, and to Professor H. Vonach for his continued interest in this work and constructive suggestions regarding the model calculations.

[1] S. M. Qaim, in *Proceedings of the International Conference on Nuclear Data for Science and Technology*, Gatlinburg, 1994, edited by J. K. Dickens (American Nuclear Society, LaGrange Park, IL, 1994), p. 186.
[2] M. Faßbender, A. F. Novgorodov, F. Rösch, and S. M. Qaim, Radiochim. Acta **65**, 215 (1994).
[3] F.-O. Denzler, F. Rösch, and S. M. Qaim, Radiochim. Acta **68**, 13 (1995).
[4] F. Rösch and S. M. Qaim, Radiochim. Acta **62**, 115 (1993).
[5] F. Rösch, A. F. Novgorodov, and S. M. Qaim, Radiochim. Acta **64**, 113 (1994).
[6] S. Sudár and S. M. Qaim, Phys. Rev. C **53**, 2885 (1996).
[7] S. M. Qaim, G. Stöcklin, and R. Weinreich, Int. J. Appl. Radiat. Isot. **28**, 947 (1977).
[8] R. Weinreich, H.-J. Probst, and S. M. Qaim, Int. J. Appl. Radiat. Isot. **31**, 223 (1980).
[9] H. P. Graf and H. Münzel, Kernforschungszentrum Karlsruhe Report KFK-1806 (1973); EXFOR Entry B0040.
[10] R. A. Esterlund and B. D. Pate, Nucl. Phys. **69**, 401 (1965).
[11] E. A. Skakun, V. G. Batij, Yu. N. Rakivnenko, and O. A. Rastrepin, Yad. Fiz. **46**, 28 (1987) [Sov. J. Nucl. Phys. **46**, 17 (1987)]; EXFOR Entry A0338.
[12] S. Flach, Ph.D. thesis, Karlsruhe, 1976; and Kernforschungszentrum Karlsruhe Report KFK-2279, 1976.
[13] H. H. Bissem, R. Georgi, W. Scobel, J. Ernst, M. Kaba, J. Rama Rao, and H. Strohe, Phys. Rev. C **22**, 1468 (1980); EXFOR Entry A0347.
[14] L. T. Auler, A. G. da Silva, and G. W. A. Newton, J. Inorg. Nucl. Chem. **41**, 2611 (1981).
[15] S. M. Qaim, M. Ibn Majah, R. Wölfle, and B. Strohmaier, Phys. Rev. C **42**, 363 (1990).
[16] S. M. Qaim, R. Wölfle, and B. Strohmaier, Phys. Rev. C **40**, 1993 (1989).
[17] B. Strohmaier, Ann. Nucl. Energy **16**, 461 (1989).
[18] M. Uhl and B. Strohmaier, ''STAPRE-A computer code for particle induced activation cross sections and related quantities,'' Institut für Radiumforschung und Kernphysik Report IRK-76/01, 1976, unpublished, and Addenda to this report; and B. Strohmaier and M. Uhl, ''STAPRE-A statistical model code with consideration of preequilibrium decay,'' International Atomic Energy Agency Report IAEA-SMR-43, 1980, p. 313.
[19] E. H. Auerbach, Brookhaven National Laboratory Report BNL-6562, 1962.

[20] J. Rapaport, V. Kulkarni, and R. W. Finlay, Nucl. Phys. **A330**, 15 (1979).
[21] G. S. Mani, M. A. Melkanoff, and I. Iori, Commissariat à l'Energie Atomique Report CEA-2379, 1963.
[22] F. Hinterberger, G. Mairle, U. Schmidt-Rohr, G. J. Wagner, and P. Turek, Nucl. Phys. **A111**, 265 (1968).
[23] F. D. Becchetti, Jr. and G. W. Greenlees, in *Polarization Phenomena in Nuclear Reactions*, edited by H. H. Barschall and W. Häberli (University of Wisconsin Press, Madison, Wisconsin, 1971), p. 78.
[24] J. R. Huizenga and G. J. Igo, Argonne National Laboratory Report ANL-6373, 1963.
[25] L. McFadden and G. R. Satchler, Nucl. Phys. **84**, 177 (1966).
[26] C. M. Perey and F. G. Perey, At. Data Nucl. Data Tables **17**, 1 (1976).
[27] E. Gadioli, E. Gadioli-Erba, and P. G. Sona, Nucl. Phys. **A217**, 589 (1973).
[28] W. Scobel (private communication).
[29] M. Blann, OVERLAID ALICE, US ERDA Report COO-3494-29, 1976, unpublished.
[30] L. Milazzo-Colli and G. M. Braga-Marcazzan, Nucl. Phys. **A210**, 297 (1973).
[31] C. Kalbach, Z. Phys. A **287**, 319 (1978).
[32] M. J. Martin and J. K. Tuli, Nucl. Data Sheets **54**, 1 (1988); **54**, 527 (1988); **58**, 351 (1989); **60**, 835 (1990); **62**, 271 (1991); **62**, 327 (1991); **66**, 1 (1992); **66**, 347 (1992); **67**, 579 (1992); **68**, 165 (1993); **68**, 635 (1993); **70**, 1 (1993).
[33] W. Dilg, W. Schantl, H. Vonach, and M. Uhl, Nucl. Phys. **A217**, 269 (1973).
[34] J. Kopecky and M. Uhl, International Atomic Energy Agency Report INDC(NDS)-238, 1990, p. 103.
[35] A. V. Ignatyuk, G. N. Smirenkin, and A. S. Tishin, Sov. J. Nucl. Phys. **21**, 255 (1975).
[36] S. Mordechai, H. T. Fortune, and W. J. Courtney, Nucl. Phys. **A287**, 109 (1977).
[37] V. N. Levkovskij, ''Activation cross sections for nuclides of average masses ($A=40-100$) by protons and α particles with average energies ($E=10-50$ MeV),'' (Inter-Vesy, Moscow, 1991), ISBN 5-265-02732-7; EXFOR Entry A0510.
[38] M. Izumo, H. Matsuoka, T. Sorita, Y. Nagame, T. Sekine, K. Hata, and S. Baba, Appl. Radiat. Isot. **42**, 297 (1991).
[39] B. Strohmaier, Ann. Nucl. Energy **22**, 687 (1995).
[40] M. Wagner, H. Vonach, A. Pavlik, B. Strohmaier, S. Tagesen, and J. Martinez-Rico, Phys. Data **13-5** (Fachinformationszentrum Karlsruhe), 1990.